

TTUKa Single-Doppler Radar Analysis of Low-Level Tornado Structure

Timothy R. Cermak, Christopher C. Weiss, Anthony E. Reinhart, Patrick S. Skinner
Texas Tech University, Lubbock, Texas

1. Introduction

Our knowledge of tornado vortex structure is largely based off numerical and laboratory simulations (e.g., Ward 1972; Rotunno 1977, 1979; Church et al. 1979; Fiedler and Rotunno 1986; Lewellen et al. 1997, 2000; Lewellen and Lewellen 2007a,b). Although useful in allowing *in situ* measurements, complications arise in attempting to apply the results of these simulations to real-life tornado-scale vortices. A more detailed understanding of tornado vortex structure, especially near the surface, is critical for improving our mechanisms of preventing loss of life and property. Over recent decades, advances in technology have improved our ability to observe and measure near-surface tornado dynamics, the most prominent of which have been mobile Doppler radars. This particular study utilizes the 8.6 mm wavelength Texas Tech University Ka-band (TTUKa) mobile Doppler radars (Figure 1). The specifications for the TTUKa radars are listed in Table 1.



Figure 1: TTUKa-1 and TTUKa-2 at Reese Technology Center near Lubbock, TX

The use of millimeter wavelength mobile Doppler radars to observe tornado and storm-scale structure has gained momentum in recent years, owing to the finer resolution relative to larger, centimeter wavelength mobile Doppler radars. Although issues can arise regarding attenuation and maximum unambiguous range, millimeter wavelength radars provide the opportunity to resolve structures otherwise lost in lower resolution data, especially at levels close to the surface. The purpose of this study is to resolve near-surface dynamical structures in and around tornado vortices. Then, using both horizontal and vertical cross-sections and the Ground-based Velocity Track Display (GBVTD; Lee et al. 1999) technique, we can attempt to relate these observed structures to one another. An overview of the GBVTD technique is outlined in section 2. Two specific cases are examined in sections 3 and 4, and concluding remarks and topics of further research are discussed in section 5.

Transmit Frequency	35 GHz
Transmit Power	200 W peak, 100 W avg.
Transmitter Type	TWTA
Antenna Gain	56 dB
Antenna Type	Cassegrain feed, epoxy reflector
Antenna Beamwidth	0.49°*
Polarization	Linear, horizontal
Waveguide	WR-28, pressurized
PRF	Variable, up to 20 KHz
Gate spacing	15 meters*
Receiver	MDS: -118 dBm
IF Frequency	60 MHz
DSP	Sigmat RVP-9
Moments	Reflectivity, radial velocity, spectrum width

Table 1: TTUKa specifications

*upgraded in Summer 2013 to 0.33° beamwidth and 12 m gate spacing

2. GBVTD

The GBVTD technique is a single-Doppler method of retrieving axisymmetric tangential and radial velocities about a vortex center. Originally developed by Lee et al. (1999) for WSR-88D Plan-Position Indicator (PPI) observations of tropical cyclones, the technique has since been adapted for use on higher resolution mobile Doppler radar observations of tornado-scale vortices as well (e.g., Lee and Wurman 2005; Tanamachi et al. 2007; Kosiba and Wurman 2010, 2013). Results using this adaptation have been found to accurately represent ideal, axisymmetric flow in most tornado vortex scenarios.

The entire GBVTD technique involves three separate steps. The first step is to perform an objective analysis on the desired PPI sweep. Traditionally, a bilinear interpolation constant-altitude PPI (CAPPI) is used. In this study, however, we employ a two-pass Barnes objective analysis. This type of analysis allows for more control over the smoothing scale length, γ , and convergence parameter, λ_0 , values for which are determined using Pauley and Wu (1990) for guidance (Table 2). The second step involves using a simplex center-seeking algorithm (Nelder and Mead 1965) to determine the best possible vortex center by maximizing vorticity using a “walking triangle” method. This method centers a triangle about a first guess input by the user, then calculates vorticity at each triangle vertex. The vertex containing the lowest vorticity is then expanded, contracted, or reflected, and this process is repeated until vorticity reaches a specified tolerance. Finally, using the objective analysis and calculated vortex center, the GBVTD algorithm transforms the data from radar-centered polar coordinates to vortex-centered coordinates and calculates the axisymmetric tangential and radial velocity components.

Parameter	This Study	Pauley and Wu (1990)
Grid Size	3 km x 3 km	–
Grid Spacing, Δd	25 m	–
γ	0.3	0.2 – 0.4
λ_0	0.033 km	1.33 Δd

Table 2: Parameters and specifications for the two-pass Barnes objective analyses

3. 14 April 2012: Cherokee, OK

During the evening hours of 14 April 2012, a single TTUKa radar successfully deployed on a tornadic supercell ~ 3.2 km north of Cherokee, OK between 00:50:57 – 01:14:53 UTC 15 April 2012. The TTUKa captured low-level PPIs and Range-Height Indicator (RHI) vertical cross-sections through two tornadoes during a parent cell cycling period. The first tornado, rated EF1 on the Enhanced Fujita scale, remained roughly 8-10 km from the radar position (Figure 2). PPIs at a 1.0° elevation angle therefore provided horizontal cross-sections ~ 175 m AGL. The second tornado, rated EF0, passed within 3 km of the radar (Figure 3). PPIs at a 0.5° elevation angle provided horizontal cross-sections of this tornado ~ 26 m AGL. We assume in both cases that the change in beam height across the tornado diameter is negligible.

Only one TTUKa was in position for this intercept, so an alternating PPI/RHI scanning strategy had to be used to obtain information on the horizontal and vertical structure. For this strategy, the radar used low-level PPIs to determine the location and direction in which the tornado was moving, then picked an RHI azimuth ahead of the tornado and scanned continuously until the tornado passed across that azimuth. This process was then repeated until the tornado either dissipated or moved out of range.

Although this strategy most accurately allows a single radar to collect both PPI and RHI cross-sections of a tornado, it eliminates the possibility of comparing simultaneous scans. Because of this, neighboring PPIs must be used for these comparisons, with typical scan-to-scan time differences around one minute.

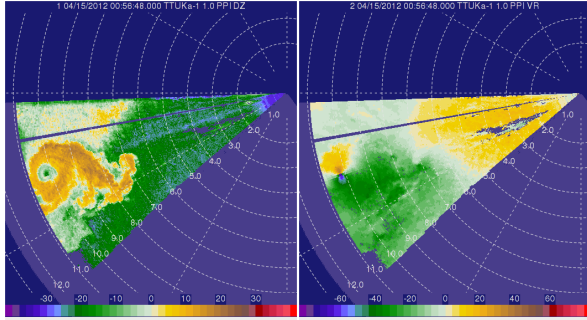


Figure 2: 0056:48 UTC 1.0° PPI, showing reflectivity (left, dBZ) and radial velocity (right, $m s^{-1}$)

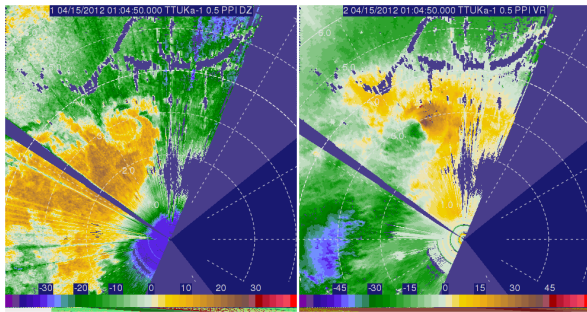


Figure 3: 0104:50 UTC 0.5° PPI, showing reflectivity (left, dBZ) and radial velocity (right, $m s^{-1}$)

Initial GBVTD-derived radial profiles of tangential velocity suggest for both tornadoes a wind profile similar to that of an ideal Burgers-Rott vortex (Burgers 1948; Rott 1958), as opposed to the more traditional Rankine-combined vortex model (Rankine 1901). The prominent difference between these two idealized vortices can be seen at the radius of maximum winds. Where a Rankine-combined vortex exhibits a discontinuity at this location, the Burgers-Rott vortex suggests a more continuous peak, which has been more commonly observed in

actual tornado vortices. Radial profiles of tangential velocity for the 0056:48 UTC PPI in Figure 2 and 0104:50 UTC PPI in Figure 3 are provided in Figure 4.

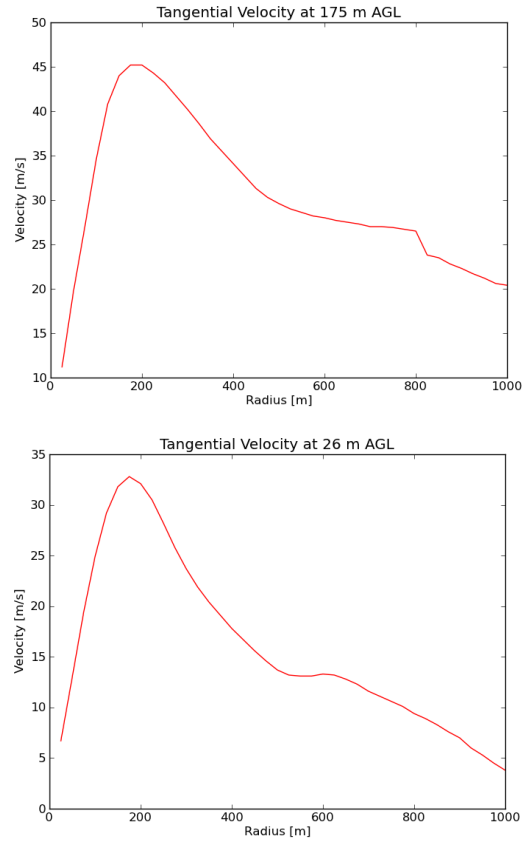


Figure 4: GBVTD-derived radial profiles of tangential velocity ($m s^{-1}$) from 0056:48 UTC (top) and 0104:50 UTC (bottom)

The retrieval of radial and tangential velocities allows for the further calculation of other important variables when considering vortex mode and stability. One of these variables is vertical vorticity, which can be calculated using the simple equation:

$$\zeta = \frac{\partial V}{\partial r} + \frac{V}{r}$$

where V is tangential velocity and r is radius. From this calculation, we can plot radial profiles of vertical vorticity (Figure 5).

Vertical vorticity, maximized at the vortex center, decreases to zero outside the radius of maximum winds without the occurrence of other local vorticity maxima. This is expected for single-celled vortex structure. These analyses match with visual records of single-celled structure during the TTUKa deployment.

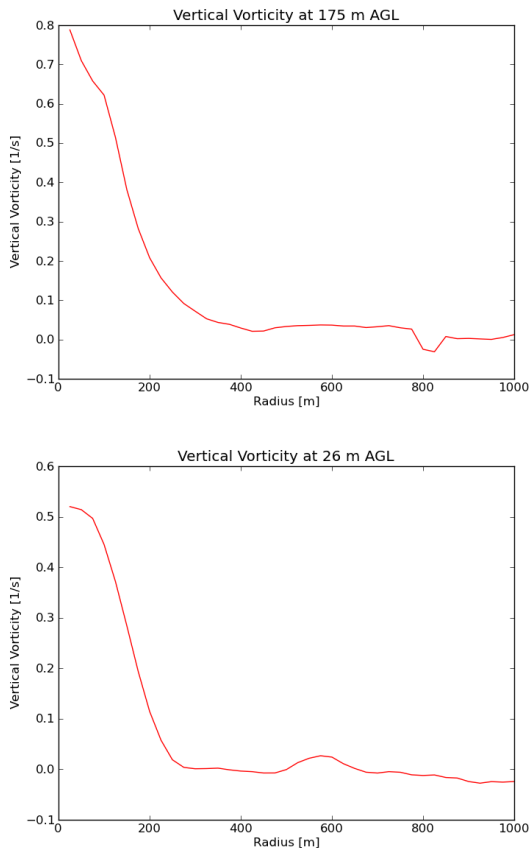


Figure 5: Radial profiles of vertical vorticity (s^{-1}) for 0056:48 UTC (top) and 0104:50 UTC (bottom)

More interesting features noted in the 14 April 2012 RHI cross-sections were the transient horizontal vorticity maxima manifesting along the outer edges of the tornado vortex (Figure 6). As can be expected, a strong horizontal shear zone is expected in that region, where a strong tornado core updraft borders the weaker, ambient vertical motions of the atmosphere. Most of these vorticity maxima appeared to

be induced by this region of strong shear. A strong, horizontal circulation exhibited opposite signs of rotation during this case (Figure 6, circled). However, this circulation was well outside the tornado ($\sim 1-2$ km), so it is unlikely induced by shear associated with the tornado. It is possible that storm-scale baroclinic or shear processes induced this horizontal vortex, or that it is the result of a complex wind field involving two simultaneous tornadoes within 3 km of each other (Figure 2). More data regarding the wind field and thermodynamic properties of the parent storm in this region are needed for further conclusions to be made.

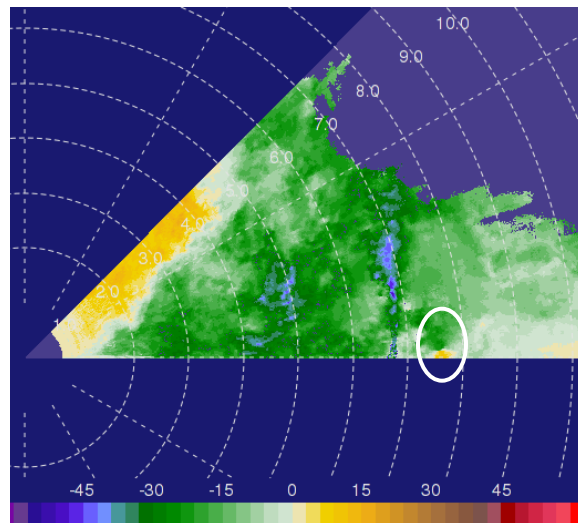


Figure 6: 0101:54 UTC RHI showing radial velocity ($m s^{-1}$). A strong horizontal vortex (see text) is circled.

4. 18 May 2013: Rozel, KS

Between 0021:46 – 0049:08 UTC 19 May 2013, a single TTUKa radar deployed approximately 1.2 km north of the intersection of US-183 and KS-156, successfully capturing low-level PPIs and RHIs through an EF4 tornado passing just west of Rozel, KS. While the tornado was roughly 9-10 km west of the TTUKa

deployment site, 0.5° and 1.0° PPIs were able to resolve horizontal cross-sections of the tornado at ~ 83 m and ~ 165 m AGL, respectively (Figures 7 and 8). It is again assumed that the change in elevation of the radar beam across the diameter of the tornado is negligible. After these initial surveillance scans, the TTUKa switched into RHI mode, capturing multiple vertical cross-sections of the tornado throughout its life (Figure 8).

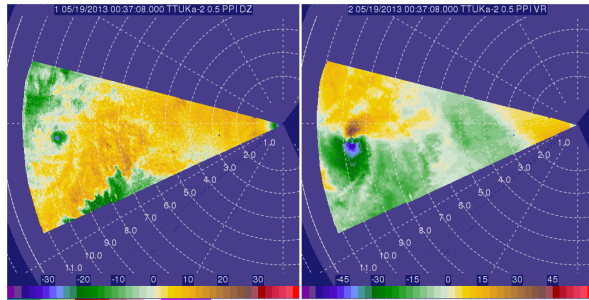


Figure 7: 0037:08 UTC 0.5° PPI, showing reflectivity (left, dBZ) and radial velocity (right, $m s^{-1}$)

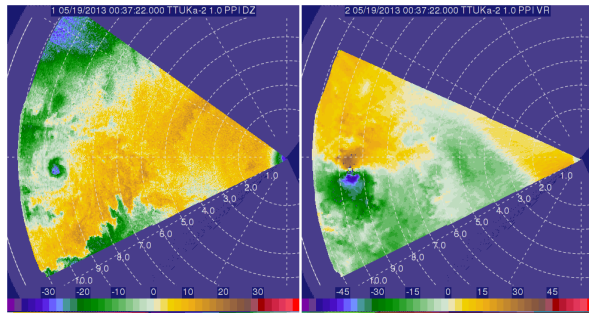


Figure 8: 0037:22 UTC 1.0° PPI, showing reflectivity (left, dBZ) and radial velocity (right, $m s^{-1}$)

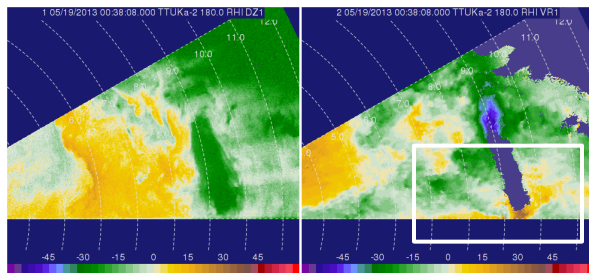


Figure 9: 0038:08 UTC RHI, showing reflectivity (left, dBZ) and radial velocity (right, $m s^{-1}$)

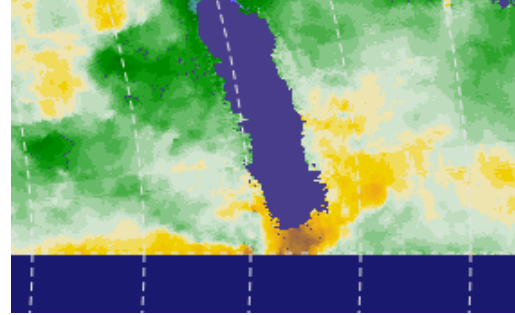


Figure 10: Zoomed in 0038:08 UTC RHI region represented by a white box in Figure 8.

The first important structure to discuss stands out in the 0038:08 UTC RHI (Figures 9 and 10). In this cross-section, a shallow, sloping inflow layer is visible in the regions surrounding the tornado vortex, close to the surface. This inflow layer ranges in depth from ~ 70 m near the tornado to ~ 250 m farther away. A narrowing inflow band can be expected regarding tornado inflow, as air from a more broad, outside circulation accelerates inward and downward towards the largest pressure perturbations near the surface and inside the tornado core. It is thought that the acceleration of air as it nears the corner flow region, where the air turns sharply upwards into the core updraft of the tornado, aids in the horizontal stretching of the inflow layer.

The corner flow region is thought to influence the intensity and structure of tornadoes. The height of this region varies greatly from case to case, and even during the life cycle of a single tornado. Few studies have attempted to quantify the height of this region, one example being Lewellen et al. (2000). The Lewellen et al. (2000) study suggests a relationship in which the corner flow depth is approximately 0.2 times the core radius. Metzger (2011) tested this relationship on the 5 June 2009 Lagrange, WY tornado, finding it to be a reasonable estimate of corner flow depth.

Using the GBVTD-derived tangential velocity profile (Figure 11), we estimate the

core radius to be between 350 – 400 m. Following the Lewellen et al. (2000) relationship would imply a corner flow depth of 70 – 80 m for this case, which matches roughly the observed inflow layer closest to the tornado vortex. The acceleration of air as it nears the corner flow region is also visible in this RHI, where the strongest inflow velocities are visible closest to the tornado.

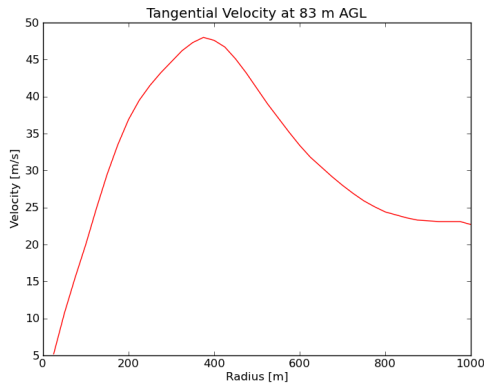


Figure 11: Radial profile of tangential velocity ($m s^{-1}$) for 0037:08 UTC

Another key feature that stands out in the 18 May 2013 case data is the multiple vortex structure later in the tornado’s life cycle. A progression of this vortex breakdown was captured through means of visual and instrumental observations. At 0037:22 UTC, the GBVTD-derived radial profile of vertical vorticity shows multiple vorticity maxima within the radius of maximum winds, at ~165 m AGL (Figure 12a). A few minutes later, around 0040 UTC, members of a scout vehicle operated by the University of Michigan took a picture of the tornado, with multiple tendril-like features extending downward from the mid-level condensation funnel clearly visible (Figure 12b). Finally, at 0042:35 UTC, an RHI vertical cross-section resolved two separate velocity maxima at the surface (Figure 12c). It is understood that vortex breakdown is a top-down process, occurring at mid levels and descending with a primary core downdraft to the surface. It is thought that

from 0037:22 – 0042:35 UTC this process was captured both instrumentally and visually by the TTUKa team.

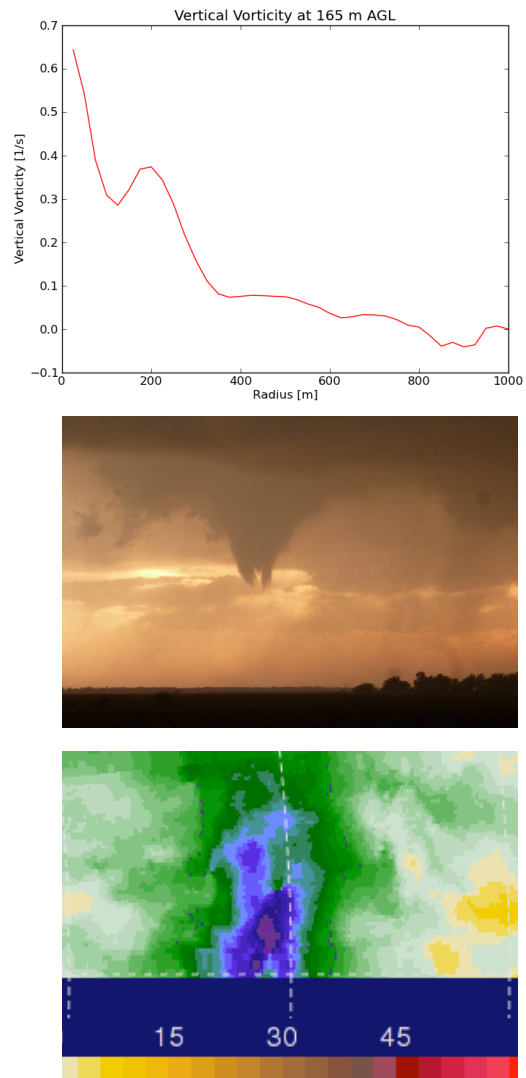


Figure 12: (a) Radial profile of vertical vorticity (s^{-1}) at 0037:22 UTC, (b) photo of tornado from 0040 UTC, (c) radial velocity ($m s^{-1}$) RHI at 0042:35 UTC

Outflow is present in the low-level GBVTD analysis (~83 m AGL) from 0037:08 UTC (Figure 13). This level is below the observed multi-celled structure in the 0037:22 UTC analyses (Figure 12). It is possible that a core downdraft from the multi-celled structure aloft reached this level,

in which case radial outflow near the tornado center would be expected. Another explanation, which has gained momentum in the research community over the past decade, could be the contamination of data by centrifuging debris. Multiple studies have looked into this (e.g., Dowell et al. 2005; Tanamachi et al. 2007; Wakimoto et al. 2012; Nolan 2013). Some studies have even attempted to quantitatively correct for this contamination (e.g., Dowell et al. 2005; Wakimoto et al. 2012), and have shown improved results in doing so during situations where debris contamination was clear. Still, the tornado during this case remained largely in open fields, only damaging a ranch house and some foliage. Moreover, the contamination would be most evident immediately outside the radius of maximum winds, where the debris is centrifuged out aloft and falls into the inflow layer. In this case, the region of outflow occurs at and inside the radius of maximum winds, suggesting debris centrifugal was not an issue, and that the downdraft associated with vortex breakdown is the primary culprit.

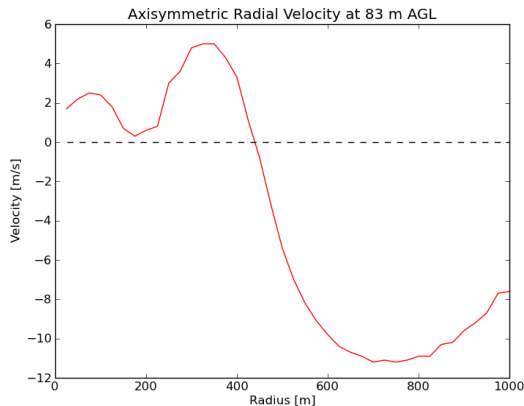


Figure 13: Radial profile of axisymmetric radial velocity ($m s^{-1}$) for 0037:08 UTC

5. Conclusions

Over recent decades, advances in technology have allowed us to more accurately measure and resolve the lowest

levels inside and immediately surrounding tornadoes. Among the most prominent of these advances have been millimeter wavelength mobile Doppler radars. The TTUKa radars used in this study are 8.6 mm wavelength single-polarization mobile Doppler radars capable of resolving structures in the near-surface tornado environment most other radars are unable to. This study focuses on the analyses and interpretations of these data, in an attempt to relate horizontal and vertical structures traditionally hypothesized to be important to tornado maintenance and intensification. Two cases were discussed, 14 April 2012 and 18 May 2013, during which a TTUKa radar successfully deployed and collected low-level horizontal and vertical cross-sections of tornadoes (Figures 2, 3, and 6-9). These data were then analyzed using the GBVTD technique (Lee et al. 1999) to retrieve both axisymmetric radial and tangential velocity about the tornado centers.

It was observed in most cases that the radial profiles of tangential velocity resembled those of an idealized Burgers-Rott vortex, instead of the traditional Rankine-combine vortex model (Figures 4 and 11). There was only one instance during which this was not true: when the tornado was going through vortex breakdown into a multi-celled structure. This process was observed during the 18 May 2013 case by utilizing both visual observation and analyzed TTUKa data (Figure 12). Both tornadoes during the 14 April 2012 case exhibited single-celled structures in the GBVTD-derived radial profiles of vertical vorticity, as well as through visual confirmation during the deployment.

A narrowing band of radial inflow was resolved in RHIs during the 18 May 2013 case. This stretching of the inflow layer is expected, as air in the broader, weaker circulation farther from the tornado accelerates downwards and into the near-

surface tornado core, where the strongest pressure perturbation exists. This region, where the air turns sharply upwards into the core updraft, is known as the corner flow region. Its depth is of increasing study over recent years, and is suspected to directly influence the strength and longevity of the tornado. We estimated the corner flow depth using suggested relationships from Lewellen et al. (2000), and found the depth to closely match the estimated inflow depth in the immediate proximity of the tornado vortex.

It is unlikely that the counter-intuitive regions of outflow inside and around the radius of maximum winds during the 18 May 2013 case were a result of contamination by debris centrifugal, since no substantial debris was observed during the deployment. Another, more likely explanation for the outflow signature involving the vortex breakdown process was also discussed. Vortex breakdown is understood to be a top-down process, and is associated with a strong core downdraft in the center of the tornado. This downdraft would therefore produce radial outflow within the radius of maximum winds, with radial inflow likely persisting beyond that point. This closely matches the radial profile of axisymmetric radial velocity (Figure 13). As previously mentioned, vortex breakdown was clearly observed at the time of these profiles. It is therefore expected that vortex breakdown is the more likely cause for the strong outflow signatures near the tornado center.

6. Acknowledgements

This study was supported by National Science Foundation grants AGS-0964088 and AGS- 0800542. The authors thank Dr. Robin Tanamachi for assistance with the GBVTD technique and the University of Michigan volunteers for helping with data collection during the Spring 2013 season.

REFERENCES

- Burgers, J. M., 1948: A mathematical model illustrating the theory of turbulence. *Adv. Appl. Mech.*, **1**, 197-199.
- Church, C. R., J. T. Snow, G. L. Baker, and E. M. Agee, 1979: Characteristics of tornado-like vortices as a function of swirl ratio: A laboratory investigation. *J. Atmos. Sci.*, **36**, 1755-1776.
- Dowell, D. C., Alexander, C. R., Wurman, J. M., and Wicker, L. J., 2005: Centrifuging of hydrometeors and debris in tornadoes: Radar-reflectivity patterns and wind-measurement errors. *Mon. Wea. Rev.*, **133**, 1501–1524.
- Fiedler, B. H., and R. Rotunno, 1986: A theory for the maximum windspeeds in tornado-like vortices. *J. Atmos. Sci.*, **43**, 2328–2340.
- Kosiba, K., and J. Wurman, 2010: The three-dimensional axisymmetric wind field structure of the Spencer, South Dakota, 1998 tornado. *J. Atmos. Sci.*, **67**, 3074–3083.
- Kosiba, K., and J. Wurman, 2013: The three-dimensional structure and evolution of a tornado boundary layer. *Wea. Forecasting*. doi:10.1175/WAF-D-13-00070.1, in press.
- Lee, W-C., B. J-D. Jou, P-L. Chang, and S-M. Deng, 1999: Tropical cyclone kinematic structure retrieved from single-Doppler radar observations. Part I: Interpretation of Doppler velocity patterns and the GBVTD technique. *Mon. Wea. Rev.*, **127**, 2419–2439.
- Lee, W-C., and J. Wurman, 2005: Diagnosed three-dimensional axisymmetric structure of the Mulhall tornado on 3 May 1999. *J. Atmos. Sci.*, **62**, 2373–2393.
- Lewellen, W. S., D. C. Lewellen, and R. I. Sykes, 1997: Large-eddy simulation of a tornado's interaction with the surface. *J. Atmos. Sci.*, **54**, 581–605.

- Lewellen, D. C., W. S. Lewellen, and J. Xia, 2000: The influence of a local swirl ratio on tornado intensification near the surface. *J. Atmos. Sci.*, **57**, 527–544.
- Lewellen, D. C., and W. S. Lewellen, 2007a: Near-surface vortex intensification through corner flow collapse. *J. Atmos. Sci.*, **64**, 2195–2209.
- Lewellen, D. C., and W. S. Lewellen, 2007b: Near-Surface Intensification of Tornado Vortices. *J. Atmos. Sci.*, **64**, 2176–2194.
- Metzger, R. S., 2011: An analysis of the structure of four tornadoes observed by Ka-band radar during the VORTEX2 project (Masters Thesis). Texas Tech University, Lubbock, TX.
- Nelder, J. A., and R. Mead, 1965: A simplex method for function minimization. *Comput. J.*, **7**, 308–313.
- Nolan, D. S., 2013: On the use of Doppler radar-derived wind fields to diagnose the secondary circulations of tornadoes. *J. Atmos. Sci.*, **70**, 1160–1171.
- Pauley, P. M., and X. Wu, 1990: The theoretical, discrete, and actual response of the Barnes objective analysis scheme for one- and two-dimensional fields. *Mon. Wea. Rev.*, **118**, 1145–1164.
- Rankine, W. J. M., 1901: A manual of applied mechanics. 16th ed. Charles Griff and Company, 680 pp.
- Rott, N., 1958: On the viscous core of a line vortex. *Z. Angew. Math. Phys.*, **9**, 542–553.
- Rotunno, R., 1977: Numerical simulation of a laboratory vortex. *J. Atmos. Sci.*, **34**, 1942–1956.
- Rotunno, R., 1979: A study in tornado-like vortex dynamics. *J. Atmos. Sci.*, **36**, 140–155.
- Tanamachi, R. L., H. B. Bluestein, W-C. Lee, M. Bell, and A. Pazmany, 2007: Ground-based velocity track display (GBVTD) analysis of W-band Doppler radar data in a tornado near Stockton, Kansas, on 15 May 1999. *Mon. Wea. Rev.*, **135**, 783–800.
- Wakimoto, R. M., P. Stauffer, W-C. Lee, N. T. Atkins, and J. Wurman, 2012: Finescale structure of the LaGrange, Wyoming, tornado during VORTEX2: GBVTD and photogrammetric analyses. *Mon. Wea. Rev.*, **140**, 3397–3418.
- Ward, Neil B., 1972: The exploration of certain features of tornado dynamics using a laboratory model. *J. Atmos. Sci.*, **29**, 1194–1204.